Remote Sensing of Environment 205 (2018) 166–179

Contents lists available at ScienceDirect

Remote Sensing of Environment

journal homepage: www.elsevier.com/locate/rse

Characterizing the encroachment of juniper forests into sub-humid and semi-arid prairies from 1984 to 2010 using PALSAR and Landsat data

Jie Wang[a], Xiangming Xiao[a,b,*], Yuanwei Qin[a], Russell B. Doughty[a], Jinwei Dong[a], Zhenhua Zou[a]

[a] Department of Microbiology and Plant Biology, Center for Spatial Analysis, University of Oklahoma, Norman, OK 73019, USA
[b] Ministry of Education Key Laboratory of Biodiversity Science and Ecological Engineering, Institute of Biodiversity Science, Fudan University, Shanghai 200433, China

ARTICLE INFO

Keywords:
Land cover
Eastern redcedar
Phenology
Vegetation indices
Biological invasion
Ashe juniper
Biodiversity
Great plains

ABSTRACT

Over the past few decades, wide encroachment of eastern redcedar (*Juniperus virginiana*) and Ashe juniper (*Juniperus ashei*) into the prairies of the U.S. Great Plains has affected wildlife habitats, forage and livestock production, and biogeochemical cycles. This study investigates the spatio-temporal dynamics of juniper forest encroachment into tallgrass prairies by generating juniper forest encroachment maps from 1984 to 2010 at 30 m spatial resolution. A pixel and phenology-based mapping algorithm was used to produce the time series maps of juniper forest encroachment using a combination of Phased Array type L-band Synthetic Aperture Radar (PALSAR) mosaic data from 2010 and Landsat 5 and 7 data (10,871 images from 1984 to 2010). We analyzed the resultant maps to understand the dynamics of juniper forest encroachment at state and county spatial scales and examined juniper occurrence by geographic region and soil type. The juniper forest maps were generated over five multi-year periods: the late 1980s (1984–1989), early 1990s (1990–1994), late 1990s (1995–1999), early 2000s (2000–2004), and late 2000s (2005–2010). We also produced a map of time since stand detection of juniper forests in 2010. Our major findings include: (1) juniper forests have expanded linearly in time at an annual rate of ~40 km^2/year since 1984; (2) juniper forests had notable spatial clusters in its expansion process; (3) ~65% of juniper forests in 2010 were < 15 years after stands have been detected; and (4) juniper forests in 2010 were mainly distributed in sandy and loamy soils with relatively low available water storage in the top soils. This study demonstrates the potential of combining a cloud computing platform (Google Earth Engine), time series optical images (Landsat), and microwave images to document the spatial-temporal dynamics of juniper forest encroachment into prairies since the 1980s at the regional scale. The results can be used to study the causes, consequences, and potential future distribution of juniper encroachment, which are relevant to the sustainable management of prairie ecosystems.

1. Introduction

Woody plant encroachment (WPE) into prairies and savannas in arid, semi-arid, and sub-humid climates has been widely reported around the world in recent years (Archer et al., 2001; Saintilan and Rogers, 2015). The encroachment of juniper species into native plant communities has gained increasing attention due to its widespread expansion in the Great Plains and the western United States, which often results in negative economic and ecological effects (Anadon et al., 2014; Engle et al., 1996; Meneguzzo and Liknes, 2015). For example, the accelerated encroachment of eastern redcedar (*Juniperus virginiana* L.) has severely threatened tall and mixed grass prairies of the Great Plains and reduced the productivity of forage and livestock (Briggs et al., 2005; Engle et al., 1996; Knapp et al., 2008). Several studies also reported that the eastern redcedar encroachment in Oklahoma prairies tends to replace the dominant oak species of the Cross Timbers, a forest-prairie ecotone (DeSantis et al., 2010a; Williams et al., 2013). The altered species composition can affect ecosystem processes, including water, carbon, and nutrient cycles. For instance, juniper encroachment into tallgrass prairies reduced streamflows (Zou et al., 2016), ground water recharge (Caterina et al., 2014), and increased carbon and nitrogen pools in plants and soils (McKinley and Blair, 2008).

Understanding the drivers, impacts, encroachment dynamics, and future trends of juniper encroachment would provide insights into rangeland management and prairie sustainability (Meddens et al., 2016). However, research and practical management of juniper encroachment have been hindered by a lack of juniper maps at local to regional spatial scales over multiple decades. For example, dominant views about the causes of WPE concentrate on fire suppression, overgrazing, increasing atmospheric CO_2, and climate change (Briggs et al.,

* Corresponding author at: Department of Microbiology and Plant Biology, University of Oklahoma, 101 David L. Boren Blvd., Norman, OK 73019-5300, USA.
E-mail address: xiangming.xiao@ou.edu (X. Xiao).

https://doi.org/10.1016/j.rse.2017.11.019
Received 18 April 2017; Received in revised form 6 November 2017; Accepted 21 November 2017
0034-4257/ © 2017 Elsevier Inc. All rights reserved.

2002; Buitenwerf et al., 2012; Kulmatiski and Beard, 2013; Ratajczak et al., 2014; Wigley et al., 2010). However, explanations for these changes in plant composition are still controversial (Archer et al., 1994; Hibbard et al., 2001; Saintilan and Rogers, 2015). One reason is that these explanations are based on localized, historical descriptions or accounts that are often conflicting (Archer et al., 1994). Another reason is the variance in drivers of WPE among ecoregions (Barger et al., 2011; Saintilan and Rogers, 2015). In addition, a number of studies have aimed to understand the impacts of woody encroachment on hydrology (Caterina et al., 2014; Zou et al., 2016), carbon (Barger et al., 2011; Pinno and Wilson, 2011), and nutrient cycles (Hughes et al., 2006; McCulley and Jackson, 2012). However, most of those studies were conducted at specific sites with field experiments, and the effects of WPE on carbon and water budgets at a regional scale are poorly understood (Barger et al., 2011; Pacala et al., 2001; Zou et al., 2016). Finally, without continuous historical data at the regional scale, it is difficult to estimate the woody plant expansion rate, describe the shapes of expansion curves, and predict the density and distribution of woody plants in the future (Barger et al., 2011). The magnitude of WPE cannot be described generally, as it varies largely among geographic areas (Buitenwerf et al., 2012).

Some efforts have been made to produce juniper encroachment maps at various spatial scales based on field survey data (Engle et al., 1996; Meneguzzo and Liknes, 2015; Schmidt and Leatherberry, 1995). However, most of these studies were conducted within the sub-state scale and in one or two time periods (Meneguzzo and Liknes, 2015). Further, traditional field survey approaches are labor-intensive and cost prohibitive, making it difficult to collect enough data to accurately map the spatio-temporal distributions of the encroaching plants over large regions (Sankey and Germino, 2008). Currently, WPE maps generated from historical observations over multiple decades at regional scales are not available (Gavier-Pizarro et al., 2012; Ge and Zou, 2013).

Remote sensing offers an opportunity to quantify the spatial-temporal patterns of WPE using a set of techniques (Meddens et al., 2016; Symeonakis and Higginbottom, 2014). Previous studies mainly explored the use of very high resolution (VHR) satellite and airborne images, from sources such as the National Agriculture Imagery Program (NAIP), QuickBird, and WordView2 (Falkowski et al., 2017; Meddens et al., 2016), and aerial photographs (Briggs et al., 2007; Fredrickson et al., 2006; Smith et al., 2008; Strand et al., 2007; Weisberg et al., 2007) to map sparse trees, including juniper, pinyon-juniper, and mesquite, at semi-arid and arid grasslands in the western USA. However, these studies were confined to smaller spatial scales over a short period of time and were inhibited by insufficient VHR data. No studies have attempted to track the dynamics of WPE over a period of decades at a regional scale.

The Landsat program has recorded continuous land cover changes at consistent spatial and temporal resolutions since 1984 (Wulder et al., 2012; Wulder et al., 2008; Wulder et al., 2016). Archived Landsat time series data have been widely used to monitor long-term changes in forests, croplands, and prairies from local to national spatial scales (Dong et al., 2015; Hansen et al., 2013; Mueller et al., 2015; Zhong et al., 2014). However, woody vegetation coverage may be confused with prairies based on optical remote sensing data (Qin et al., 2016b; Shimada et al., 2014). The Japan Aerospace Exploration Agency (JAXA) provides multiple resolution datasets from the Advanced Land Observing Satellite Phased Array type L-band Synthetic Aperture Radar (ALOS/PALSAR) (Shimada et al., 2009; Shimada and Ohtaki, 2010). The L-band PALSAR can penetrate clouds and forest canopies to document forest structure (Baghdadi et al., 2009; Shimada et al., 2014). The datasets have been utilized by many studies to map forests (Qin et al., 2015; Shimada et al., 2014) and plantations (Chen et al., 2016; Dong et al., 2013; Miettinen and Liew, 2011) at regional and global scales. The combination of these two datasets provided a new approach to study the spatio-temporal dynamics of juniper forest encroachment into prairies over multiple decades (Wang et al., 2017). To date, there is a need to implement this method at the regional scale or larger spatial scales.

Encroachment of woody plants in prairies is a succession process that occurs over decades (Van Auken and Bush, 2013). With respect to the stature and canopy cover of the woody plant elements, we describe the WPE process as having four stages: grasslands, savanna grasslands, savanna woodlands, and forests. Savanna grasslands have sparse and scattered trees and shrubs, and savanna woodlands have low-density trees and shrubs (Archer et al., 2001). Forest is defined as land (> 0.5 ha) with tree canopy cover > 10% and minimum tree height of 5 m by the United Nations Food and Agriculture Organization (FAO) (FAO, 2012). Juniper forests are the focus of this study. Several scientific questions need to be addressed: (1) What is the spatial distribution and area of juniper forests in a year? (2) How many years are the juniper forests identified from satellite images? and (3) What factors drive the observed spatial pattern and temporal dynamics of juniper forests? The state of Oklahoma, USA, is chosen as a case study area for us to better understand the current and historical patterns with juniper forest encroachment into tall and mixed grass prairies during 1984–2010. The juniper in Oklahoma comprises mainly eastern redcedar and Ashe juniper (*Juniperus ashei*), which are an encroaching but native species (Engle et al., 1996). The specific objectives of this study are to: (1) generate a map of juniper forests in Oklahoma in 2010 at 30 m spatial resolution through analyses of PALSAR and Landsat images acquired in 2010, and then determine the age of the juniper forests in 2010 through analysis of time series Landsat images from 1984 to 2010; (2) quantify the spatio-temporal dynamics of juniper encroachment at the state and county level from 1984 to 2010 using juniper forest maps produced for each period; and (3) characterize the geographical patterns and soil settings of the juniper encroachment during 1984–2010 based on the resultant maps. We report the results in five multi-year periods: the late 1980s (1984–1989), early 1990 (1990–1994), late 1990s (1995–1999), early 2000s (2000–2004), and late 2000s (2005–2010).

2. Material and methods

2.1. Study area

The state of Oklahoma is in the southern Great Plains, USA (33.4°N–37.1°N, 94°W–103.2°W) consisting of 77 counties with a total land area of about 181,035 km^2 (Fig. 1). It has a temperate continental climate, where the annual mean air temperature ranges from 13 °C in the north to 17 °C in the south. The average annual precipitation ranges from ~410 mm in the northwest to ~1700 mm in the southeast according to the Parameter-elevation Relationships on Independent Slopes Model (PRISM) precipitation datasets of 1980–2010 (http://prism.oregonstate.edu/) (Fig. 1). The PRISM climate datasets are developed based on climate observations from weather stations, and more information can be found in previous publications (Daly et al., 2008; Daly et al., 2015). Elevation ranges from ~100 m to ~1500 m above sea level according to the 30 m Shuttle Radar Topography Mission Digital Elevation Model (SRTM/DEM) (Fig. S1a). Oklahoma's diverse soil types have a wide range of texture from clay to sand. According to the 2011 National Land Cover Database (2011 NLCD), grasslands, croplands, deciduous forest, and pasture/hay are the main land cover classes and account for 36%, 18%, 17%, and 11% of the total area, respectively (Fig. S1b). Evergreen forests occupy 3% of the total land area, mostly distributed in the southeast and dominated by pine plantations. The deciduous forests are mostly dominated by oak tree species (Diamond and Elliott, 2015).

Level I and level II ecoregion classifications from the U.S. Environmental Protection Agency (USEPA) (https://www.epa.gov/eco-research/ecoregions-north-america) were used to ecologically and geographically characterize the forest and prairie assemblages of natural communities and species in Oklahoma (Fig. 1). The broad ecological classification is temperate forest in the east and prairie in the west.

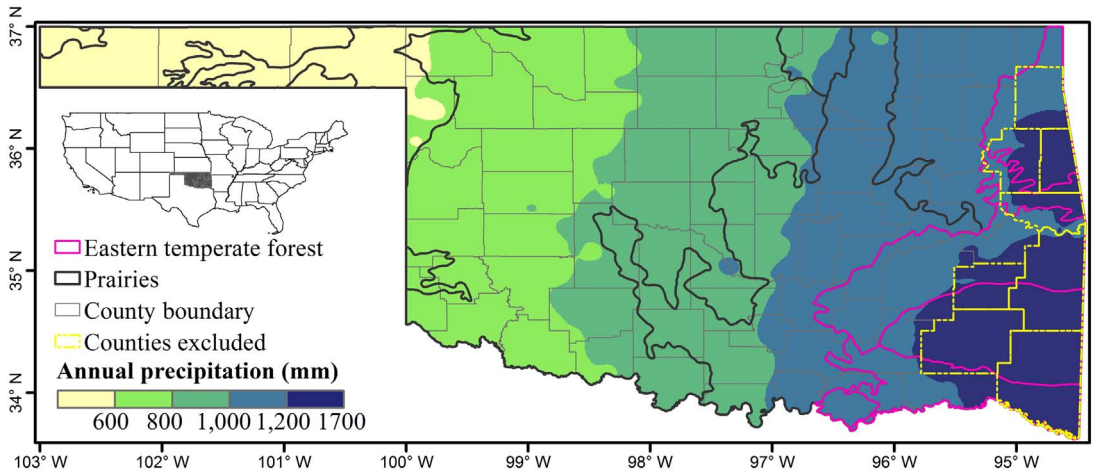

Fig. 1. Ecoregions, annual precipitation and counties of Oklahoma, inset figure denotes the location of Oklahoma within the United States. The eight counties located in eastern temperate forest ecoregion with high annual precipitation were not included in the study area.

The forest region covers several eastern counties and has relatively high annual precipitation. The prairie region covers a majority of Oklahoma and has relatively low annual precipitation. There are three primary sub-ecoregions (level III) in this prairie area; from east to west they are the: Cross Timbers, Central Great Plains, and High Plains and Southwestern Tablelands of the panhandle region. Field surveys indicated that juniper species had widely encroached on the Cross Timbers and especially the Central Great Plains (Coppedge et al., 2001; DeSantis et al., 2011; Williams et al., 2013). Eastern redcedar is the main encroaching juniper species, followed by Ashe juniper. Redberry juniper (*J. pinchotii*) and other juniper species (*J. monosperma* and *J. scopulorum*) are distributed only locally within Oklahoma (Engle et al., 1996). Juniper encroachment into prairies is the focus of this study, so we selected the counties within the prairie ecoregion and the transition zone between prairies and eastern forests. The transition zone consists of the counties located in the western portion of Eastern Temperate Forest ecoregion that has relatively low annual precipitation. We excluded eight eastern counties located in the Eastern Temperate Forest ecoregion that have relatively high annual precipitation (Fig. 1).

2.2. Data

2.2.1. PALSAR 25 m orthorectified image data

The 25 m PALSAR orthorectified mosaic datasets from 2007 to 2010 at Fine Beam Dual (FBD, HH, HV) polarization mode were generated from data acquired between the months of June and October (Shimada et al., 2014). The HH and HV backscatter data were processed by geometric correction and radiometric calibration (Shimada et al., 2009; Shimada and Ohtaki, 2010). We downloaded all of the 25 m PALSAR orthorectified mosaic data for Oklahoma in 2010 from the Earth Observation Research Center, JAXA (http://www.eorc.jaxa.jp/ALOS/en/palsar_fnf/fnf_index.htm). The Digital Number (DN) values (amplitude) of HH and HV were converted into backscattering coefficients (gamma-naught) in decibels using the following calibration coefficient (Shimada et al., 2009).

$$\gamma^o = 10 \times \log_{10} < DN^2 > + CF \tag{1}$$

where γ^o is the backscattering coefficient in decibels; DN is the digital number value of pixels in HH or HV; and CF is the absolute calibration factor of − 83.

2.2.2. Landsat data and pre-processing

We processed all available surface reflectance products of Landsat 5 and 7 accessible in the Google Earth Engine (GEE), a cloud computing platform. The surface reflectance data were generated from the Landsat Ecosystem Disturbance Adaptive Processing System (LEDAPS) through radiance calibration and atmospheric correction (Masek et al., 2006; Vermote et al., 1997). The study area is covered by 23 Landsat path/rows (Fig. S1a). We collected a total of 14,086 Landsat 5 and 7 images from January 1984 to March 2011 to construct a 3-dimensional data cube of land surface reflectance. Fig. S2 shows the annual distributions of all available Landsat TM/ETM + surface reflectance data over the study period by sensors (Landsat 5 and 7) (Fig. S2a), by Landsat path/row (Fig. S2b), and by month (Fig. S2c).

We evaluated the observation quality of the 3-D data cube at the pixel level in two steps. First, the bad observations (clouds, cloud shadows, snow/ice, and scan-line corrector (SLC)-off gaps) were identified as NODATA according to the Fmask (Zhu and Woodcock, 2012) and metadata. Then, we tabulated the number of good observations for individual pixels during each whole year and each winter (December, January, and February) (Fig. S3). Figs. S3 and S4 show the spatial distribution and frequency histogram of the observation quality of the time series Landsat data cube.

We used the surface reflectance data with good observations to calculate the Normalized Difference Vegetation Index (NDVI) (Tucker, 1979) and Land Surface Water Index (LSWI) (Xiao et al., 2005). We used the times series data of NDVI and LSWI to analyze the vegetation phenology, as NDVI is related to vegetation greenness and LSWI is sensitive to leaf and soil water (Xiao et al., 2006).

$$LSWI = \frac{\rho_{NIR} - \rho_{SWIR}}{\rho_{NIR} + \rho_{SWIR}} \tag{2}$$

where ρ_{NIR} and ρ_{SWIR} are the surface reflectance values of near-infrared (760–900 nm) and shortwave-infrared bands (1550–1750 nm).

2.2.3. Oklahoma ecological system map

This study used the Oklahoma Ecosystem Map (OKESM), which presents the statewide vegetation cover (Diamond and Elliott, 2015). The OKESM product was generated from multiple datasets including remote sensing, digital soils, slope, and streams using a decision tree classification approach. Remote sensing images between December 2010 and August 2011 were used for the map in the eastern regions, and images between April 2013 and January 2014 were used to map the western regions. A user's accuracy of 85% was reported for this product (Diamond and Elliott, 2015). This dataset can be downloaded freely from the Oklahoma department of wildlife conservation website (http://www.wildlifedepartment.com/facts_maps/ecoregions.htm).

2.2.4. Soil survey geographic database

Soil is a primary environmental factor that influences ecosystem

stability in many regions (Maestas et al., 2016). We examined the physical and hydrological properties of soils to identify the soil environments favoring juniper encroachment, including soil texture (% sand, silt, clay), soil depth to restrictive layer for crop roots (crop root zone depths) (Staff, 2016a), and available water storage (AWS) at four depths: 0–25 cm, 0–50 cm, 0–100 cm and 0–150 cm. The 10 m gridded Soil Survey Geographic (gSSURGO) database for Oklahoma was downloaded from the United States Department of Agriculture (USDA) (Staff, 2016b). This soil data product contains information about soil components and properties collected by the National Cooperative Soil Survey. We resampled this product by the nearest neighbor method to 30 m to match the spatial resolution of the juniper maps.

2.3. Mapping algorithms

2.3.1. Algorithms of juniper forest mapping

This study aims to document the historical distributions of juniper forests. Juniper is a type of evergreen tree. Therefore, we developed an algorithm composed of three sequential mapping steps including forest map, evergreen forest map, and juniper forest map, as shown in the workflow (Fig. S5). The following paragraphs describe the algorithm development for each step and a summary of the juniper forest mapping.

We used the forest definition of the FAO as land (> 0.5 ha) with tree canopy cover > 10% and minimum tree height of 5 m (FAO, 2012). Forests have a different backscatter signature than other land cover types (e.g. grasslands, croplands, water, etc.) in HH, HV, HH/HV (Ratio), and HH-HV (Difference) that can be used to identify forests (Qin et al., 2015; Qin et al., 2016a). Previous studies have developed a decision classification algorithm for forest mapping based on 50 m PALSAR mosaic data (Dong et al., 2012) and the integrated data of 50 m PALSAR and MODIS (Qin et al., 2015; Qin et al., 2016b). In this study, we produced the forest map of Oklahoma (Forest-2010) using 25 m PALSAR data from 2010 following the decision rule of $16 < HV < -8$, and $2 < Difference < 8$, and $0.3 < Ratio < 0.85$, which is documented in detail in a previous study in Oklahoma (Qin et al., 2016a). This Forest-2010 map serves as a baseline forest map and is overlaid with the time series Landsat data to identify and map evergreen forests based on their phenology characteristics in the next mapping step.

Evergreen forests keep green leaves throughout a year, while deciduous forests shed leaves in winter. Green leaves have higher reflectance in the NIR band than SWIR band, which results in positive LSWI. In contrast, senescent leaves and soil have lower NIR reflectance than SWIR, which produces negative LSWI. A simple algorithm of $LSWI > 0$ for all good observations in a whole year was developed to separate evergreen forest from deciduous in tropical regions (Xiao et al., 2009). This algorithm has been successfully implemented to map evergreen forests in temperate regions (Qin et al., 2016b). With respect to the mixed forest pixels, this algorithm identified them as either evergreen or deciduous forests depending on which signal is stronger (Qin et al., 2016b). In this study, the Landsat-derived LSWI time series of eastern redcedar, Ashe juniper, and deciduous forests at site level suggested the applicability of this method to extract evergreen forests in Oklahoma (Fig. 2). According to this algorithm, we counted the number of $LSWI > 0$ in all the good observations within a year as the frequency of $LSWI > 0$ (FrqLSWI) for individual forest pixels. Forest pixels that meet the criteria of $FrqLSWI \geq 0.9$ were identified as evergreen forests. Here, we modified the threshold of 1.0 used in early studies (Qin et al., 2016b; Xiao et al., 2009) to 0.9 to identify the potential maximum evergreen forest area and thus reduce the omission of evergreen pixels caused by short term disturbances (e.g., drought). We used this method to produce the annual evergreen forest maps (AEFMs) based on the Forest-2010 and the Landsat images in each year over 1984–2010. These AEFMs were used to identify juniper forests in the next step.

Phenology analysis of greenness-based Landsat-derived NDVI time series revealed that eastern redcedar and Ashe juniper had significantly lower VIs in summer and higher VIs in winter than did deciduous forest (Fig. 2). We analyzed the monthly mean NDVI ($NDVI_{mean}$) at the regional scale using training region of interests (ROIs) of eastern redcedar, Ashe juniper, and deciduous forests (Fig. S6a) based on Landsat 5 and 7 images from 2009 to 2010. The monthly $NDVI_{mean}$ time series (Fig. S6b) suggested that the $NDVI_{mean}$ in winter is more able to separate juniper trees from deciduous species, as the monthly $NDVI_{mean}$ of juniper in winter reached higher values than deciduous forests. This study extracted juniper forests based on the winter $NDVI_{mean}$ using a threshold of 0.4 in accordance with the method proposed in our recent publication (Wang et al., 2017). A statistical analysis of the winter $NDVI_{mean}$ spectral signature suggested the 0.4 threshold can separate 95% of eastern redcedar pixels (> 0.4) from 99% pixels of other trees (< 0.4) (Wang et al., 2017). We followed the criteria of winter season, $NDVI_{mean} > 0.4$, to identify the juniper forests from the AEFMs for each year during 1984–2010.

In this study, we first generated the juniper forest map in 2010 following the three mapping steps. Then, the annual juniper forest maps during 1984–2009 were produced using the same method. We combined these annual juniper forest maps into five multi-year periods using frequency combination to reduce uncertainties caused by image quality or other factors (e.g. drought). The five periods comprised the late 1980s (1984–1989), early 1990s (1990–1994), late 1990s (1995–1999), early 2000s (2000–2004) and late 2000s (2005–2010). During each period, we tabulated the number of individual pixels identified as juniper based on the annual juniper forest maps. A pixel with a number ≥ 3 (frequency ≥ 50%) was identified as juniper forest for each period. As a result, we reported the juniper forest map in 2010 representing the latest status of juniper forest encroachment and the historical juniper forest maps in five periods. With respect to this algorithm, due to lack of long-term PALSAR data, we produced a forest map using 2010 PALSAR data, which was used as a baseline to map the historical juniper forests. After all, this method, detecting the historical juniper forests within the extent of 2010 forest, could miss some juniper forests that existed in the early periods but were removed by various control efforts (e.g., cleared or burned) before 2010.

2.3.2. Regional implementation of the juniper forest mapping algorithm

Although forests in central and western Oklahoma have been historically dominated by deciduous species, some non-juniper evergreen species can become established in this region. These evergreen species may cause uncertainties in the implementation of the juniper forest mapping algorithm. Therefore, we generated a non-juniper evergreen forest mask from the 10 m OKESM dataset. We merged the pine plantation classification with shortleaf pine forest and other evergreen forest (non-juniper and non-pine) from the OKESM and resampled it to 30 m to match the resolution of the Landsat images using the nearest neighbor method (Fig. S7). In this study, the final juniper forest encroachment maps for 2010 and five periods were generated after masking out the non-juniper evergreen forests.

2.3.3. The stand age of juniper forests in 2010 – number of years identified as juniper forest

Stand ages of juniper forests are useful indicators for juniper encroachment over time, but it is difficult to estimate stand age when it is defined according to the first year that a few juniper trees established in a prairie. In this remote sensing study, the stand age of juniper forests in 2010 is defined as number of years a juniper forest pixel in 2010 (based on PALSAR and Landsat images in 2010) has been detected as forest using time series Landsat images in 1984–2009. Hereafter, the term *time since stand detection* is used in this remote sensing study. We mapped the time since stand detection of juniper forests in 2010 at pixel level based on the resultant maps in 2010 and the five periods. For each juniper forest pixel in 2010, we detected the first year of juniper forest

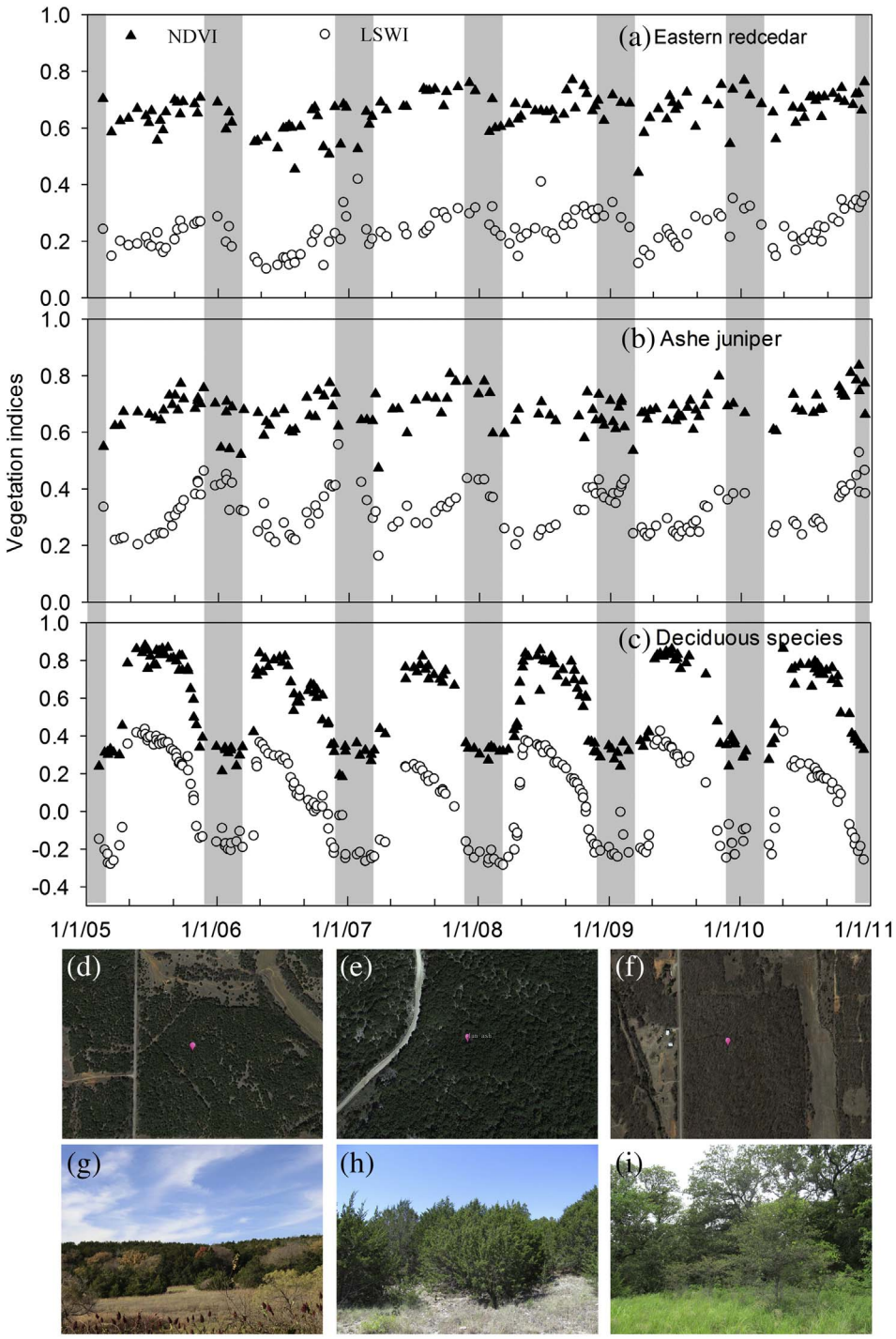

Fig. 2. (a, b, c) time series of vegetation indices, (d, e, f) the landscapes in Google Earth images, and (g, h, i) field photos of eastern redcedar, Ashe juniper and deciduous species, respectively.

occurrence from the historical juniper forest maps in five periods, and defined as ≤ 5 (first year as juniper forest in 2005–2010), ≤ 10 (2000–2004), ≤ 15 (1995–1999), ≤ 20 (1990–1994), and ≥ 20 years old (first year as juniper forest in 1984–1989). We repeated this process for all juniper pixels to generate the time since stand detection map of juniper forests in 2010.

2.4. Accuracy assessment and comparison

The stratified random sampling method was used to collect the ground reference ROIs for the accuracy assessment (Olofsson et al., 2014). First, we generated random points in each stratum of juniper forest (250 points) and other land cover types (including 250 non-juniper forest points and 600 non-forest points) based on the OKESM map. Second, 100 m square buffers (> 0.5 ha) were generated according to the random points. Finally, these random square buffers were overlaid with the VHR images in Google Earth (GE). These GE images clearly depict the land cover patterns on the ground and are usually used as reference data in the land cover classifications based on moderate or coarse spatial resolution data (Beckschafer, 2017; Mueller et al., 2015). Using GE images for winters during 2009–2011, we selected 180 ROIs which fit the definition of juniper forests as validation samples. Similarly, we checked the ROIs of non-juniper forests and non-forest types using the GE images as a reference. In this procedure, the ground samples, which were used to validate the forest map in Oklahoma in our recent publication (Qin et al., 2016a), were used as an

auxiliary reference. We obtained 218 non-juniper forest ROIs covering deciduous and non-juniper evergreen forests, and 570 non-forest ROIs covered cropland, grassland, water, and other land cover types. Fig. S8 shows the spatial distribution of the validation ROIs we collected for juniper forest, non-juniper forest, and non-forest land cover types in 2010. These ROIs (including 2437 juniper forest pixels and 8742 other land cover pixels) were used to calculate the confusion matrix to assess the accuracy of the juniper forest map in 2010 following the best practices described by Olofsson et al. (2014).

We selected the vegetation classes related to the juniper species from OKESM to produce the juniper woodland/forest map (OKESM-JWF). We aggregated the 10 m OKESM-JWF map (binary 0 and 1) into a 30 m OKESM-JWF percentage map. We compared the 2010 juniper forest map (PALSAR/Landsat-JF2010) with the OKESM-JWF map in terms of the pixel-based spatial agreement and total area at the county level.

2.5. Spatio-temporal dynamic analysis of juniper encroachment

We analyzed the spatio-temporal dynamics of the juniper forest area and stand age at state and county scales. The total area and mean stand age of the juniper forest were calculated at each spatial scale. To understand the geographical patterns of juniper encroachment, we further examined the juniper area dynamics by (1) geographic regions divided by latitude (0.1° interval), longitude (0.1° interval), and elevation (50 m interval); and (2) the soil physical and hydrological properties including texture, depth, and AWS.

3. Results

3.1. The juniper forest map in 2010

We sequentially produced the Oklahoma maps of forest (Fig. S9), evergreen forest (Fig. S10), and juniper forest (Fig. 3) in 2010. The resultant juniper forest map in 2010 (PALSAR/Landsat-JF) suggests that juniper encroachment in Oklahoma has not occurred uniformly in space. Extensive juniper encroachment occurred mainly in western and central Oklahoma forming three encroachment clusters (labeled 1, 2, and 3 in Fig. 3). The western encroachment cluster included Woodward, Dewey, Major, Blaine, Canadian and Caddo counties. The northcentral encroachment cluster mainly covered Logan, Payne, and Pawnee counties. The southcentral cluster covers Murray, Johnston and Marshall counties. This juniper forest map had an overall accuracy (OA) of 0.96 ± 0.004 and the juniper forest category had producer's accuracy (PA) of 0.89 ± 0.01 and user's accuracy (UA) of 0.95 ± 0.009 (Table 1). This product showed good spatial consistency about the juniper forest distribution with the OKESM-JWF map (Fig. S11a, b). The comparison between these two products was shown in Supporting Information.

3.2. Area dynamics and time since stand detection of juniper forests

Fig. 4a–e show the juniper forest maps during five periods from the late 1980s to the late 2000s, with an interval of five or six years. Fig. 4f summarizes the juniper forest area for each period. Juniper forest area increased from ~350 km^2 in the late 1980s to ~500 km^2 during the early 1990s. In the late 1990s, juniper forest expanded continuously, and the area increased to ~800 km^2. In the early and late 2000s, the area reached ~1100 km^2 and ~1300 km^2, respectively. During 1984–2010, the increase in juniper forest area was strongly linear with an encroachment rate of ~48 km^2 per year ($P < 0.001$) at the state level. The dynamics of juniper forest encroachment during two consecutive periods were shown in detail in Fig. S12.

Fig. 5 shows the time since stand detection map of the juniper forests in 2010. This map is composed of ages 1–5 (~24%), 6–10 (~22%), 11–15 (~18%), 16–20 (~15%), and > 20 (~21%) years old. Approximately 64% of the juniper forests in 2010 had a detected time < 15 years, reflecting the juniper forests were detected after the

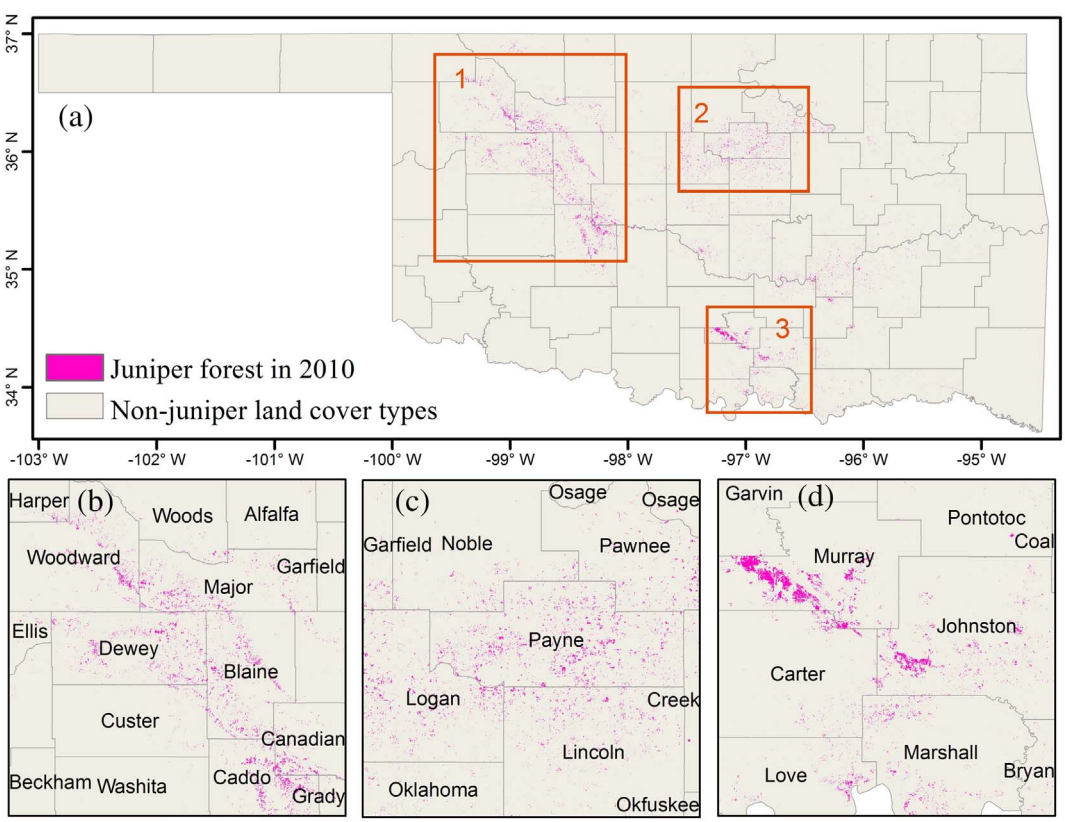

Fig. 3. (a) the juniper forest map in 2010 and (b, c, d) are three zoom-in views for the case regions labeled as 1,2,3 in (a), respectively.

Table 1
Estimated error matrix of juniper forest map in 2010 based on the validation regions of interests (ROIs) from Google Earth images and field photos. User's (UA), Producer's (PA) and Overall (OA) accuracy are shown in the table. Accuracy measures are presented with a 95% confidence interval.

		Reference			UA	PA	OA
		Juniper	Non-juniper	Total			
Map	Juniper	0.25	0.01	0.26	0.95 ± 0.009	0.89 ± 0.010	0.96 ± 0.004
	Non-juniper	0.03	0.71	0.74	0.96 ± 0.004	0.98 ± 0.003	
	Total	0.28	0.72				

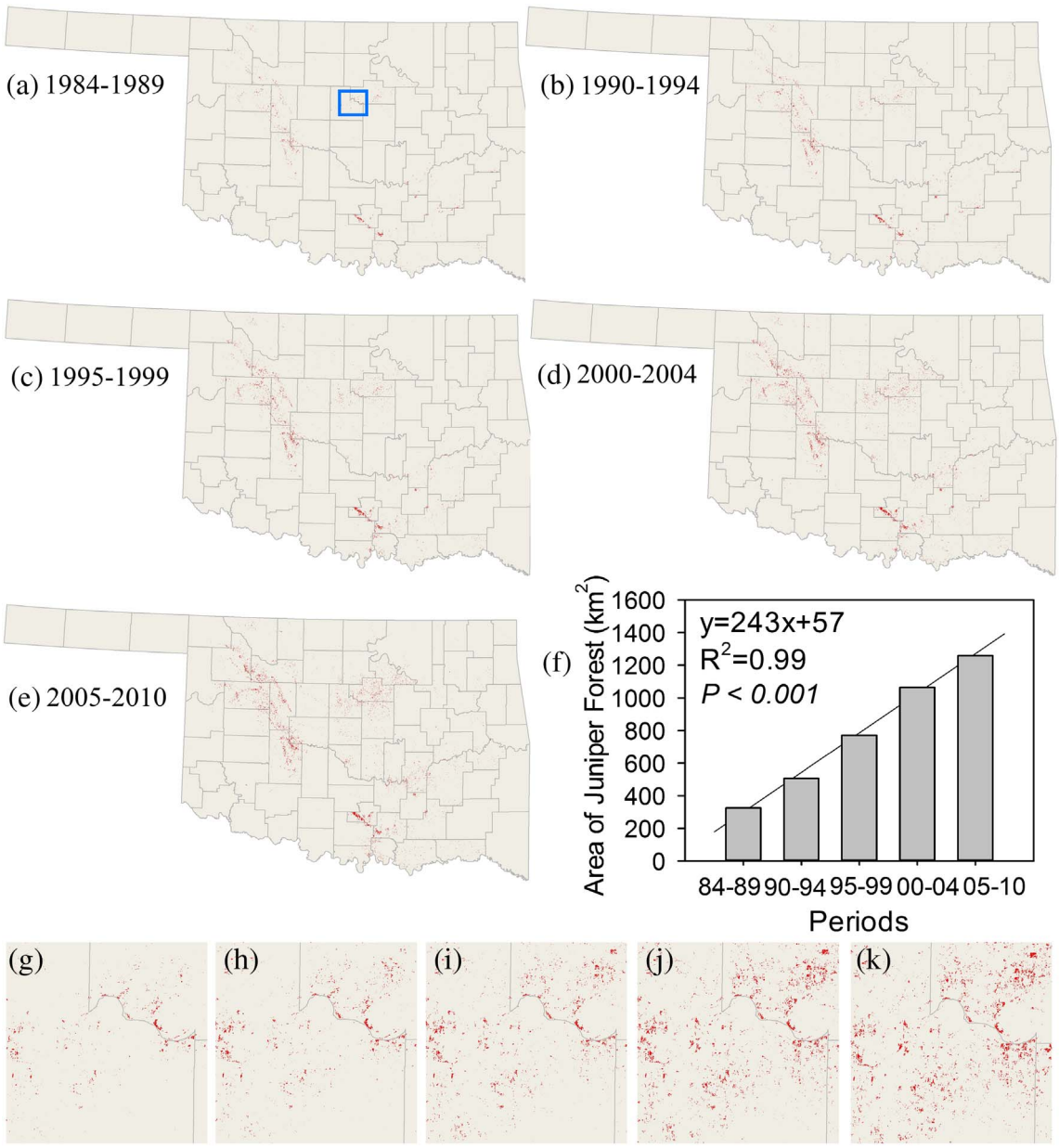

Fig. 4. (a–e) Spatial distribution of juniper forests at five periods during 1984–2010. (f) shows the juniper forest area in each period. (g–k) shows the zoom-in views from the resultant juniper forest maps of five periods for the region highlighted by the blue box in (a). (For interpretation of the references to color in this figure legend, the reader is referred to the web version of this article.)

late 1990s. Juniper stands of 20 years or older comprise 21% of the total, which demonstrates the juniper forests were formed and detected prior to the 1990s. Collectively, times since stand detection suggest that the juniper in Oklahoma is still young at present.

The historical juniper forest maps demonstrate that the counties of Oklahoma have experienced various degrees of juniper encroachment. The juniper area in the five study periods and the mean time since stand detection in 2010 were calculated for each county (Fig. S13). Total land area is different for each county in Oklahoma, so we standardized the juniper forest area of each county using a ratio of the juniper forest area to the total county land area in each time period. This ratio provides more reasonable comparisons of juniper encroachment at the county

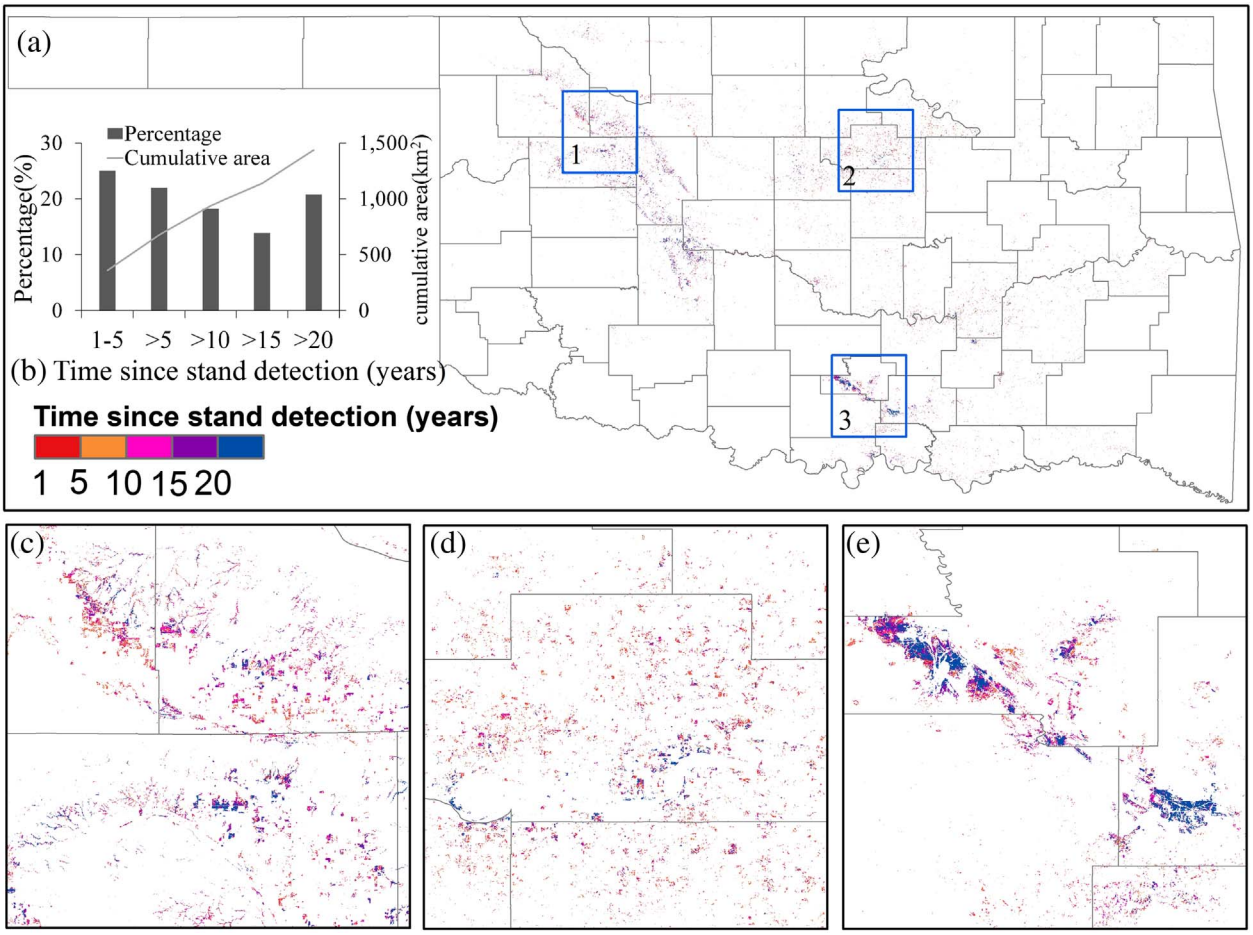

Fig. 5. (a) time since stand detection of juniper forests in 2010 and (b) the histogram distribution. (c, d, e) are three zoom-in views from the time since stand detection map in (a) for case regions labels as 1, 2, 3, respectively.

level. Fig. 6 shows that the western and central counties experienced the most substantial encroachment of juniper (e.g. Payne, Dewey, Blaine, and Murray). Payne and Murray counties had the greatest juniper encroachment during 1984–2010, with the average annual juniper forest encroachment occupying > 0.1% of the county land areas (Fig. S14). The mean time since stand detection of the juniper forests in 2010 ranged from 5 to 18 years at the county level (Fig. S13). In 2010, twenty-five counties had mean juniper forest stand ages < 10 years, 8 counties had mean stand ages larger than 15 years, and the remaining 36 counties between 10 and 15 years.

3.3. Geographic characteristics of juniper forest encroachment

The geographic characteristics of juniper forest encroachment were investigated along longitude, latitude, and elevation gradients (Fig. 7). From west to east, the juniper forests were mainly concentrated between − 100° E to − 98° E and − 97.5° E to − 95° E (Fig. 7a). From the late 1980s to the late 2000s, these two regions had a comparable distribution of juniper forests and rate of encroachment. For example, in the late 1980s the total juniper coverage was 160 km^2 for both regions, and in the late 2000s, the area expanded to 570 km^2 and 590 km^2 for the west and east regions, respectively. The juniper forest encroachment rate was about 18 km^2 per year for both regions. We noted that the juniper forest encroachment was very small at ~98° W. It could be attributed to the extensive cover of croplands at this region (Fig. S1b) and juniper trees cannot easily encroach into agricultural ecosystems with extensive human management.

In terms of latitudinal patterns, juniper encroachment was concentrated in three regions with latitudes of 33.7° N–34.6° N, 34.6° N–35.7° N and 35.7° N–37° N. Juniper encroachment varied along latitude gradients (Fig. 7b). During 1984–2010, the region within 35.7° N–37° N experienced the fastest rate of juniper encroachment, followed by the central region between 35° N–35.7° N and the lower region within 33.7° N–35° N.

There are two clear regions of juniper encroachment following an elevation gradient from 90 m to 750 m (Fig. 7c). A threshold of about 300 m can be used to divide juniper encroachment into low elevation and high elevation clusters. Both clusters experienced notable juniper encroachment from 1984 to 2010. In the late 1980s, the area proportions were 41% and 58% for high and low clusters, respectively. These proportions changed to 44% and 56% in the late 2000s. Trend analysis (Fig. S15) showed the juniper forests had significant positive trends within the cluster regions along with longitude, latitude, and elevation during the five study periods. The majority of intervals had P value < 0.01 (Fig. S15).

3.4. The potential role of soils in juniper forest encroachment

Soil water potential, content, and available water storage (AWS) varies among different soil types and affects tree and grass competition. Therefore, we examined the relationships between juniper forest encroachment and soil texture, depth, and AWS during 1984–2010 (Figs. 8 and 9). In Oklahoma, juniper forest encroachment occurred more frequently on soils of sand and loam than clay soils (Fig. 8). Based on the available soil texture data, juniper cover was highest in sandy loam soils throughout the entire study period of 1984–2010 (Fig. 8f) and these soils experienced the highest rate of juniper forest encroachment demonstrated by a trend analysis (P < 0.01) in Fig. S16.

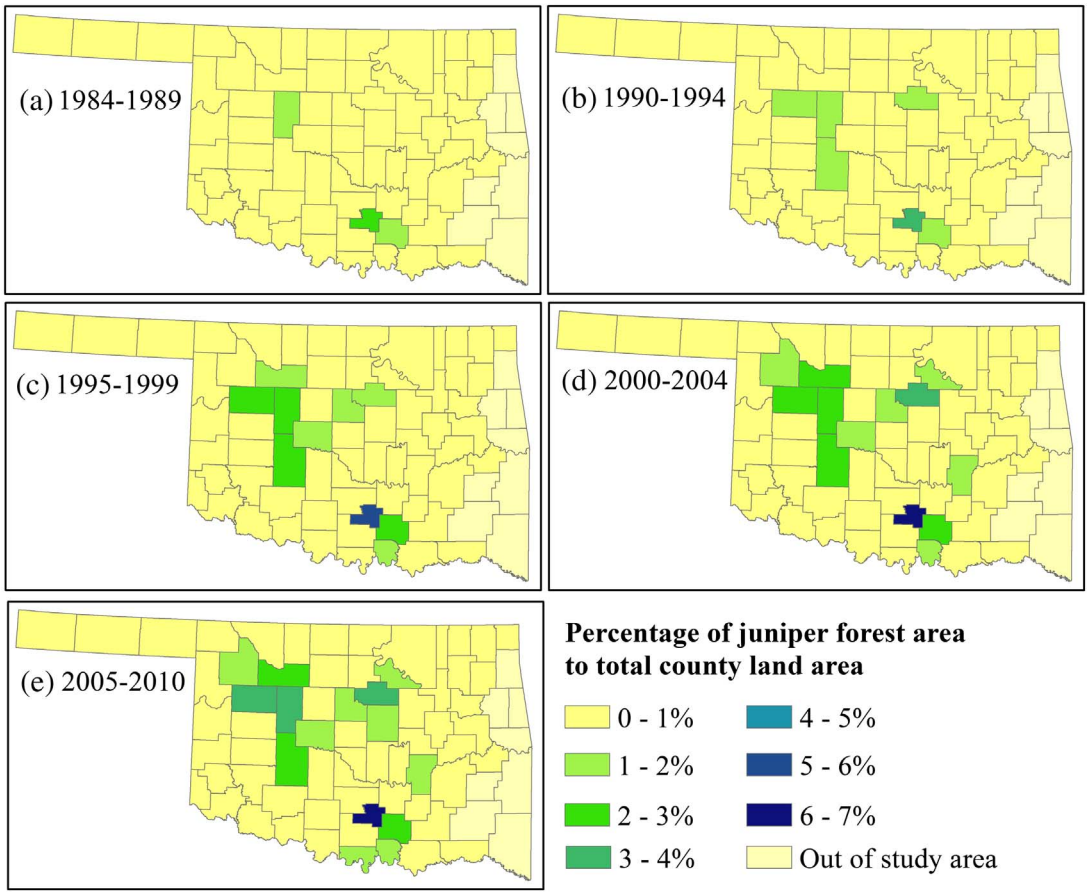

Fig. 6. Dynamics of the percentage of the juniper forest area to the total county land area in five historical periods.

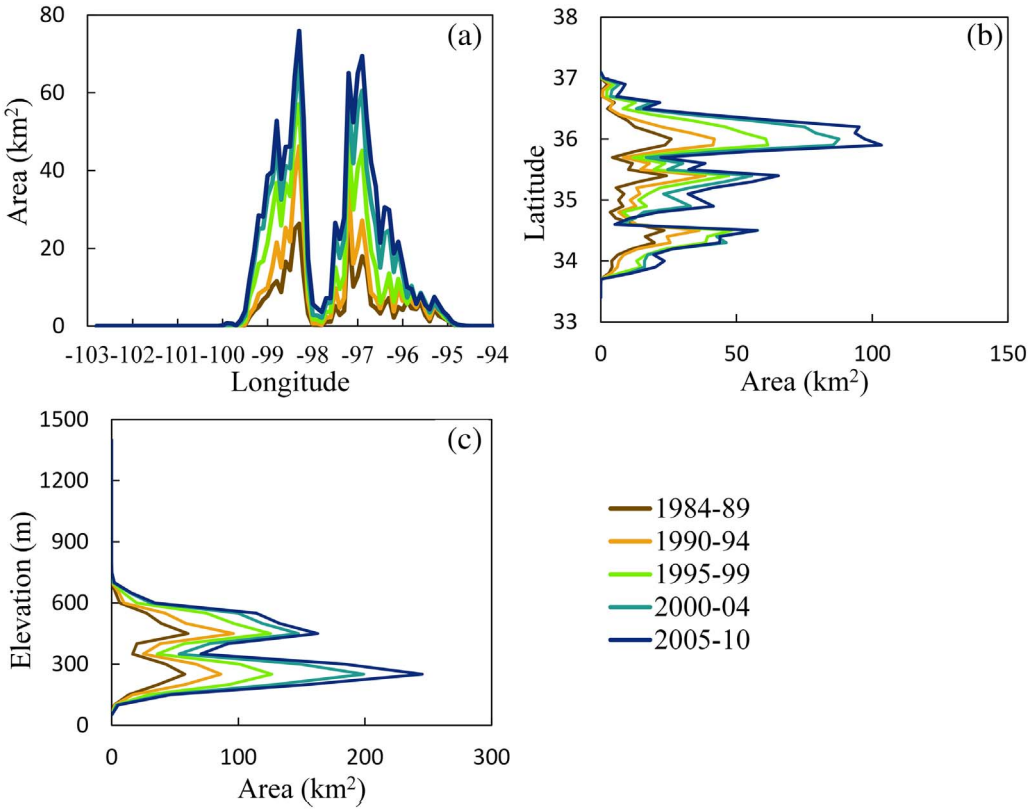

Fig. 7. Area dynamics in five periods analyzed by geographic regions of longitude, latitude and elevation.

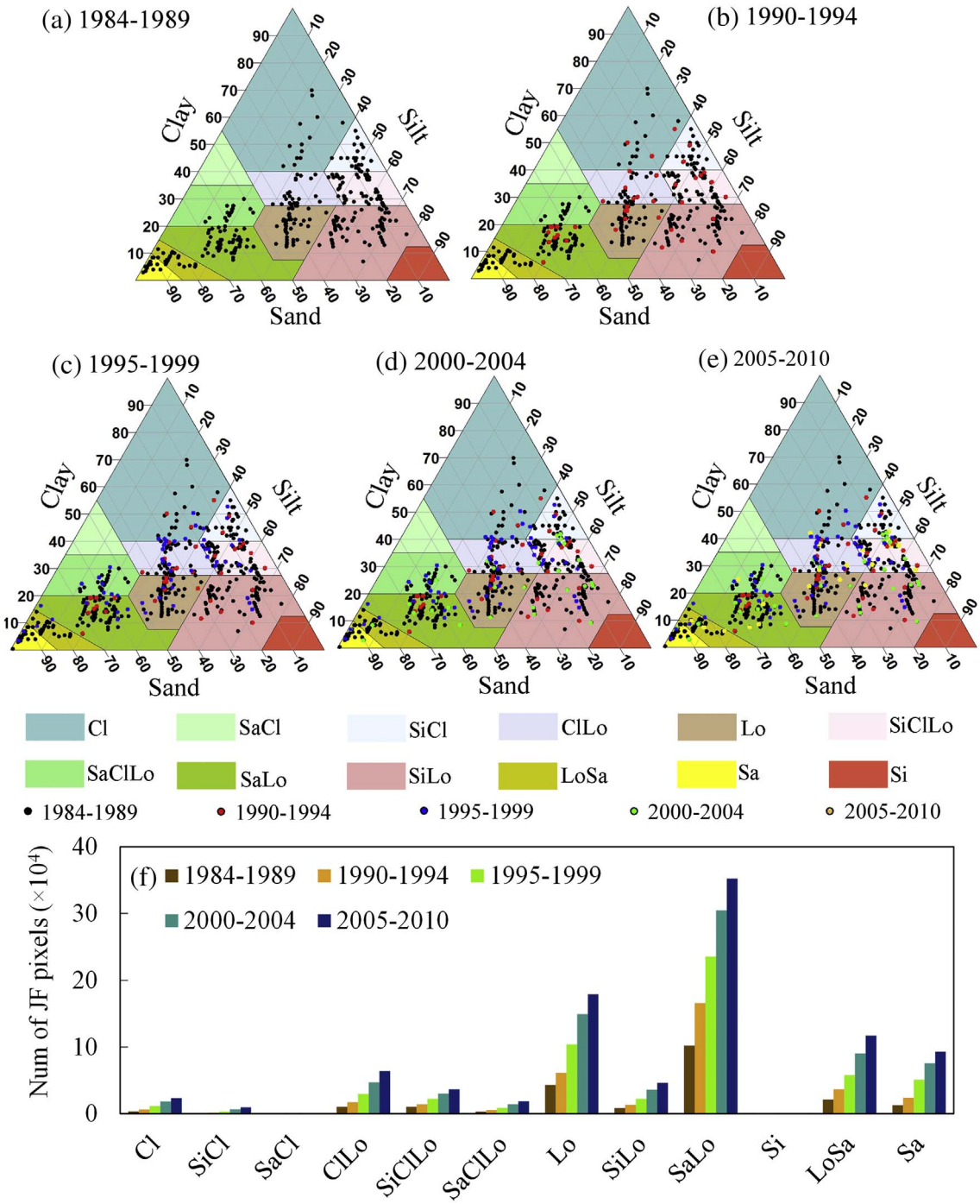

Fig. 8. (a–e) Juniper forest pixel distribution at different soil texture in five historical periods. The color of the points shows the period of first detection. The background used the soil classification system of USDA, including clay (Cl), silty clay (SiCl), sandy clay (SaCl), clay loam (ClLo), silty clay loam (SiClLo), sandy clay loam (SaClLo), loam (Lo), silty loam (SiLo), sandy loam (SaLo), silt (Si), loamy sand (LoSa), and sand (Sa). (f) number of juniper forest pixels (num of JF pixels) at each soil type in five periods.

Fig. 9a shows that juniper encroachment occurred widely on various soil depths in Oklahoma during 1984–2010. After the late 1990s, the regions with soil depth > 100 cm had more juniper than did the regions with lower soil depth. Fig. 9b–e shows the percentages of juniper forest area during five periods estimated based on soils characterized by AWS from the top soil (0 cm) to different depths of 25 cm, 50 cm, 100 cm and 150 cm. This result suggests more juniper encroachment occurred in the soils with lower AWS in the top soils (Fig. 9b–e). Trend analysis showed that the soils with lower AWS also experienced a fast encroachment rate ($P < 0.01$) over the study period (Fig. S17). The selectivity of juniper to the soil environment may provide insights into where juniper encroachment may occur in the future.

4. Discussion

4.1. Spatio-temporal dynamics of juniper forest encroachment

The resultant maps clearly show that juniper forests expanded continuously at the state level and that the encroachment varied significantly at the county level. Our results were consistent with the findings of the early field surveys (Engle et al., 1996). Geographical analysis suggested juniper encroachment expanded along latitudinal

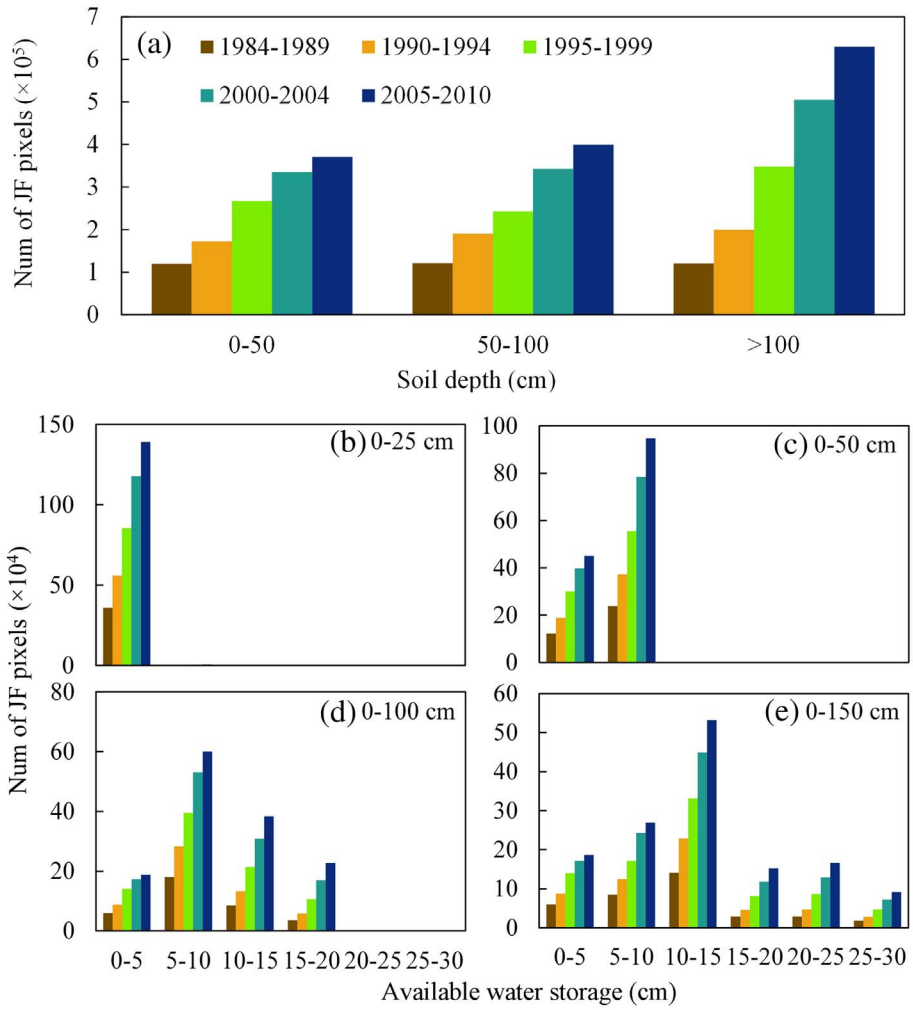

Fig. 9. (a) The number of juniper forest pixels (num of JF pixels) at different soil depths during five periods. We used crop root zone depths to indicate soil depths, as these depths are generated according to the root-limiting criteria. (b, c, d, e) Juniper forest encroachment in different soil types examined by Available Water Storage from the top soil (0 cm) to different depths of 25 cm (0–25), 50 cm (0–50), 100 cm (0–100) and 150 cm (0–150), respectively.

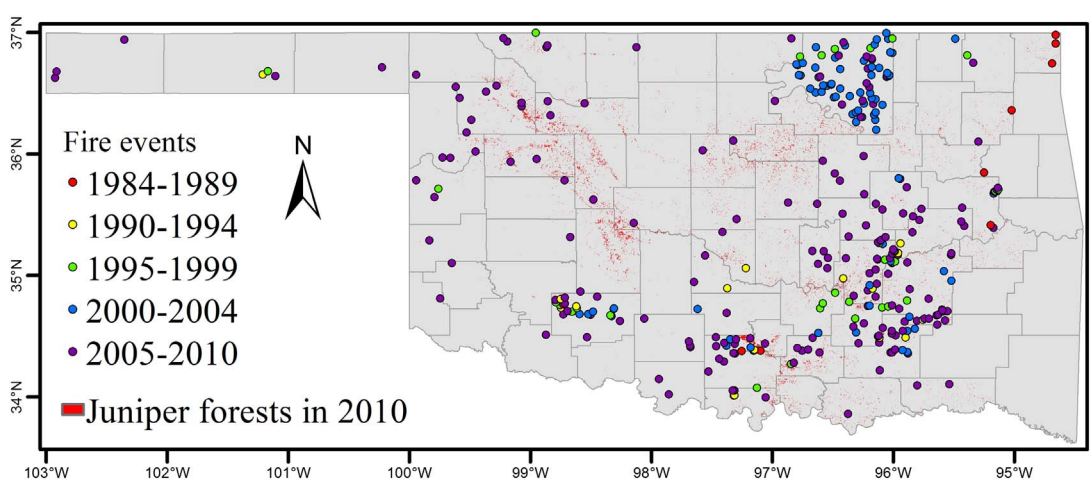

Fig. 10. The fire occurrence in Oklahoma during 1984–2010 and the juniper forests in 2010. Each point presents a fire event and different color shows the period of the fire event. Here, we used the fire occurrence dataset from the program of Monitoring Trends in Burn Severity (MTBS) (https://www.mtbs.gov/).

and longitudinal gradients to northern and western regions in Oklahoma. This result concurs with observations made by other studies, in that woody plants around the world have expanded latitudinally and that woody encroachment is occurring in water-limited prairies (Saintilan and Rogers, 2015). Fire plays an important role on the structure of grassland ecosystem (Belsky, 1992). Studies on historical fire regimes suggested that decrease of fire frequency allowed the rapid establishment of juniper species on the North American prairies (DeSantis et al., 2010b; DeSantis et al., 2011; Jones and Bowles, 2016). The comparison between juniper forest map in 2010 and the fire occurrence during 1984–2010 suggested that the resultant map reasonably described the juniper forests occurring in the regions with few or no fire events (Fig. 10).

Our results demonstrate the increase of juniper forest area during

the 2000s are in agreement with the findings by Meneguzzo and Liknes (2015) on eastern redcedar forest expansion in eight states of the central United States in 2005 and 2012 based on forest inventory and analysis data. Their study showed that Nebraska increased the most with ~600 km^2 and followed by Kansas with ~210 km^2. The annual increases in eastern redcedar forests ranged from −3 km^2 in South Dakota to ~85 km^2 in Nebraska. Our study estimated that juniper forest expanded ~200 km^2 in Oklahoma from the early to the late 2000s at a rate of ~40 km^2/year, which is about half the rate calculated for Nebraska and slightly higher than the rate of expansion in Kansas at ~30 km^2/year. Although juniper encroachment varies greatly among counties in Oklahoma, most of the counties had a similar encroachment magnitude (Fig. S14) with the reported annual rate of 2% for the eastern redcedar expansion in the Loess Canyons region of Lincoln County, Nebraska (Walker and Hoback, 2007).

We noticed some discrepancies in area estimates between our remote sensing-based study and the early field survey results in Oklahoma. A survey by the Soil Conservation Service assessed that eastern redcedar and Ashe juniper had expanded from about 6070 km^2 in 1950 to 14,164 km^2 by 1985 in Oklahoma (Engle et al., 1996). The invaded area was estimated to be > 16,187 km^2 by 1989 (Grumbles, 1989) and over 24,281 km^2 reported by a survey in 1994 (Engle et al., 1996). These numbers were acquired through questionnaire responses from each Natural Resources Conservation Service (NRCS) field office in Oklahoma. Respondents encircled the regions having > 50 eastern redcedar or Ashe juniper trees per acre on a map of their county (~10 trees per pixel of Landsat) (Engle et al., 1996). These surveys used a classification system based on the number of trees without considering the canopy coverage and height. In contrast, our study focused on the dynamics of the juniper forests extracted from remote sensing images according to the forest definition by the FAO as lands with tree canopy coverage > 10%. Therefore, the juniper forest maps produced in this study did not illustrate young or sparse juniper in savanna grasslands or savanna woodlands where the definition of forest was not met. In addition, the estimated accuracy of the field survey results, generated by using questionnaire responses, is unknown. The discrepancy between our results and early field survey reports could be explained by the different classification systems and methodologies.

4.2. Juniper encroachment with soil features

In addition to the dominant explanations for WPE (e.g. fire suppression, overgrazing, elevated CO_2), some studies proposed that prior drought and increasing precipitation intensity drive WPE into prairies through changing soil water (Kulmatiski and Beard, 2013; Ward et al., 2014). Our study suggested that there had been substantial spatial heterogeneity in juniper forest encroachment during 1984–2010 in Oklahoma (Figs. 4, S13). More encroachment occurred in the central and northwestern counties. The inconsistent encroachment of juniper into native ecosystems could be attributed to multiple factors. The results of this study provide some remote-sensing evidence that drought may cause a rapid increase of eastern redcedar in Oklahoma, which is a drought-tolerant species that is able to compete with shallow rooted grasses during drought (DeSantis et al., 2011; Lassoie et al., 1983). A literature review showed soil water is a factor controlling woody shrub encroachment into the mesic prairies (Saintilan and Rogers, 2015). A field experiment in a sub-tropical savannah ecosystem revealed increased precipitation intensity facilitated WPE (Kulmatiski and Beard, 2013). Soil moisture availability is regulated by precipitation, soil properties, and geomorphology (Eagleson and Segarra, 1985). Likewise, soil available water storage influences the partitioning of precipitation and the effect of water stress on plants during long drought periods (Weng and Luo, 2008). Grasses and trees have different root systems, so the competition between them is affected by soil water availability (Wang et al., 2016). Our study reveals that juniper is concentrated more in sand and loam than clay soils and favors soils with relatively low available water storage. These studies suggest soil properties may be associated with the spatially uneven encroachment of juniper in Oklahoma. For example, one study in the Mojave Desert showed soil attributes moderate long-term plant responses to climate (Munson et al., 2015). Additional studies are required to evaluate the roles of soil in juniper encroachment on the tall and mixed grass prairies in Oklahoma.

4.3. The uncertainty of juniper forest maps

The uncertainties on the historical juniper forest distribution in the resultant maps could be caused potentially by data quality and algorithm implementations at the regional scale across complex landscapes. Previous studies suggested some challenges in land cover mapping include the inconsistent quality of input images at temporal and spatial scales (Gong et al., 2013; Hansen et al., 2016). In this study, data quality analysis at the pixel level showed that good observational data had notable inter-annual variations and ~10% of the pixels did not have good quality data during the winter seasons from 1984 to 1991 (Fig. S4). The uneven availability of Landsat images could cause some uncertainties in the annual juniper forest maps. To alleviate the potential uncertainties, this study combined the annual juniper forest maps into multi-year products using a frequency composition method.

The potential commission errors could be caused during the application of the phenology-based algorithm for juniper forest mapping. Although this algorithm was developed based on the juniper-specific phenological feature of green foliage in winter, some non-juniper evergreen species such as live oak (*Quercus virginiana* and *Q. fusiformis*) might have had similar phenological features and spectral signatures to juniper. To reduce such potential uncertainty, this study produced a non-juniper evergreen forest map from the OKESM as a mask in the regional implementation of algorithms. However, it is uncertain about the accuracy of this mask to depict the non-juniper evergreen species over the study period. In addition, this study used Forest-2010 as a basic forest extent to trace back the historical juniper forests due to availability of PALSAR data in 2010. The resultant maps of juniper forests do not include those juniper forests that were removed before 2010.

4.4. Implications and future work

At present, there remains uncertainty regarding the drivers of WPE and predicting its consequences and distribution in the future (Van Auken, 2009; Williams et al., 2013; Wine et al., 2012). The results of this study provide new spatial-temporal data as a foundation for improving these relevant studies from local to regional scale. For example, previous studies showed that hydrological processes of a mesic prairie in the north-central Oklahoma changed because of eastern redcedar encroachment by reducing stream flow, groundwater recharge, and changing soil hydraulic properties (Caterina et al., 2014; Wine et al., 2012; Zou et al., 2014). These studies were carried out at experimental sites located in the Payne County, Oklahoma. A study using the field samples from eight forest sites across the central and western Oklahoma found that eastern redcedar encroachment reduced litter quality and altered soil microbial communities in the upland oak forests (Williams et al., 2013). According to our resultant maps, these studies selected reasonable study sites located in the regions experiencing juniper forest encroachment. However, the conclusions were obtained at the site level. The resultant juniper forest encroachment maps could be used as input to make the relevant studies performed at the state level within a continuous space. We will execute these studies in the future.

With respect to the mapping of juniper encroachment, this study well documented the historical dynamics of juniper forest encroachment using images from Landsat and PALSAR. Our work did not map the sparse or young juniper trees within the stages of savanna grasslands and savanna woodlands during the WPE process. The areas in the

early stages of the juniper encroachment process will turn into juniper forests in the future as tree density, canopy and height increase. Therefore, it is necessary to estimate the juniper encroachment within the early stages of tree and grass mixture (savanna grasslands and savanna woodlands) using very high resolution images (e.g. NAIP, Worldview 3) in the future studies, which will certainly improve our understanding and ability to predict future juniper encroachment in the drylands.

5. Conclusions

Woody plants are rapidly encroaching on multiple ecosystems, causing many negative effects on water and nutrients cycles, rangeland management, and biodiversity conservation. Long-term juniper encroachment maps were unavailable at the regional scale, limiting our ability to understand the spatial and temporal dynamics of juniper encroachment and predict encroachment trends. Our study facilitates this problem-solving by developing a pixel and phenology-based algorithm to map juniper forests in Oklahoma from 1984 to 2010 by using 14,086 Landsat 5 and 7 images and PALSAR data. We generated juniper forest maps for five historical periods during 1984–2010. Based on these maps, we analyzed the spatial dynamics of encroachment at state and county spatial scales and characterized the juniper encroachment by geographic region and soil environment. In addition, the stand age of the juniper forests in 2010 was examined to indicate the status of encroachment in Oklahoma. Further studies are needed to examine the drivers and potential consequences of juniper encroachment using the produced juniper forest maps.

Acknowledgments

This study was supported by research grants through the USDA National Institute of Food and Agriculture (NIFA) (2013-69002 and 2016-68002-24967) and the US National Science Foundation EPSCoR program (IIA-1301789). We thank Sarah Xiao at Yale University for English editing of the manuscript. We thank the anonymous reviewers for their constructive comments and suggestions for improving this manuscript.

Appendix A. Supplementary data

Supplementary data to this article can be found online at https://doi.org/10.1016/j.rse.2017.11.019.

References

Anadon, J.D., Sala, O.E., Turner, B.L., Bennett, E.M., 2014. Effect of woody-plant encroachment on livestock production in North and South America. Proc. Natl. Acad. Sci. U. S. A. 111, 12948–12953.
Archer, S., Vavra, M., Laycock, W., Pieper, R., 1994. Woody plant encroachment into southwestern grasslands and savannas: rates, patterns and proximate causes. In: Ecological Implications of Livestock Herbivory in the West. Society for Range Management, pp. 13–68.
Archer, S., Boutton, T.W., Hibbard, K.A., 2001. Trees in grasslands: biogeochemical consequences of woody plant expansion. In: Global Biogeochemical Cycles in the Climate System, pp. 115–138.
Baghdadi, N., Boyer, N., Todoroff, P., El Hajj, M., Begue, A., 2009. Potential of SAR sensors TerraSAR-X, ASAR/ENVISAT and PALSAR/ALOS for monitoring sugarcane crops on Reunion Island. Remote Sens. Environ. 113, 1724–1738.
Barger, N.N., Archer, S.R., Campbell, J.L., Huang, C.Y., Morton, J.A., Knapp, A.K., 2011. Woody plant proliferation in North American drylands: a synthesis of impacts on ecosystem carbon balance. J. Geophys. Res. Biogeosci. 116.
Beckschafer, P., 2017. Obtaining rubber plantation age information from very dense Landsat TM & ETM plus time series data and pixel-based image compositing. Remote Sens. Environ. 196, 89–100.
Belsky, A.J., 1992. Effects of grazing, competition, disturbance and fire on species composition and diversity in grassland communities. J. Veg. Sci. 3, 187–200.
Briggs, J.M., Knapp, A.K., Brock, B.L., 2002. Expansion of woody plants in tallgrass prairie: a fifteen-year study of fire and fire-grazing interactions. Am. Midl. Nat. 147, 287–294.
Briggs, J.M., Knapp, A.K., Blair, J.M., Heisler, J.L., Hoch, G.A., Lett, M.S., McCARRON, J.K., 2005. An ecosystem in transition: causes and consequences of the conversion of mesic grassland to shrubland. Bioscience 55, 243–254.
Briggs, J.M., Schaafsma, H., Trenkov, D., 2007. Woody vegetation expansion in a desert grassland: prehistoric human impact? J. Arid Environ. 69, 458–472.
Buitenwerf, R., Bond, W.J., Stevens, N., Trollope, W.S.W., 2012. Increased tree densities in South African savannas: > 50 years of data suggests CO_2 as a driver. Glob. Chang. Biol. 18, 675–684.
Caterina, G.L., Will, R.E., Turton, D.J., Wilson, D.S., Zou, C.B., 2014. Water use of *Juniperus virginiana* trees encroached into mesic prairies in Oklahoma, USA. Ecohydrology 7, 1124–1134.
Chen, B., Li, X., Xiao, X., Zhao, B., Dong, J., Kou, W., Qin, Y., Yang, C., Wu, Z., Sun, R., 2016. Mapping tropical forests and deciduous rubber plantations in Hainan Island, China by integrating PALSAR 25-m and multi-temporal Landsat images. Int. J. Appl. Earth Obs. Geoinf. 50, 117–130.
Coppedge, B.R., Engle, D.M., Fuhlendorf, S.D., Masters, R.E., Gregory, M.S., 2001. Urban sprawl and juniper encroachment effects on abundance of wintering passerines in Oklahoma. In: Avian Ecology and Conservation in an Urbanizing World. Springer, pp. 225–242.
Daly, C., Halbleib, M., Smith, J.I., Gibson, W.P., Doggett, M.K., Taylor, G.H., Curtis, J., Pasteris, P.P., 2008. Physiographically sensitive mapping of climatological temperature and precipitation across the conterminous United States. Int. J. Climatol. 28, 2031–2064.
Daly, C., Smith, J.I., Olson, K.V., 2015. Mapping atmospheric moisture climatologies across the conterminous United States. PLoS One 10.
DeSantis, R.D., Hallgren, S.W., Lynch, T.B., Burton, J.A., Palmer, M.W., 2010a. Long-term directional changes in upland Quercus forests throughout Oklahoma, USA. J. Veg. Sci. 21, 606–615.
DeSantis, R.D., Hallgren, S.W., Stahle, D.W., 2010b. Historic fire regime of an upland oak forest in south-central North America. Fire Ecol. 6, 45–61.
DeSantis, R.D., Hallgren, S.W., Stahle, D.W., 2011. Drought and fire suppression lead to rapid forest composition change in a forest-prairie ecotone. For. Ecol. Manag. 261, 1833–1840.
Diamond, D.D., Elliott, L.F., 2015. Oklahoma Ecological Systems Mapping Interpretive Booklet: Methods, Short Type Descriptions, and Summary Results. Oklahoma Department of Wildlife Conservation, Norman.
Dong, J.W., Xiao, X.M., Sheldon, S., Biradar, C., Duong, N.D., Hazarika, M., 2012. A comparison of forest cover maps in Mainland Southeast Asia from multiple sources: PALSAR, MERIS, MODIS and FRA. Remote Sens. Environ. 127, 60–73.
Dong, J.W., Xiao, X.M., Chen, B.Q., Torbick, N., Jin, C., Zhang, G.L., Biradar, C., 2013. Mapping deciduous rubber plantations through integration of PALSAR and multi-temporal Landsat imagery. Remote Sens. Environ. 134, 392–402.
Dong, J.W., Xiao, X.M., Kou, W.L., Qin, Y.W., Zhang, G.L., Li, L., Jin, C., Zhou, Y.T., Wang, J., Biradar, C., Liu, J.Y., Moore, B., 2015. Tracking the dynamics of paddy rice planting area in 1986–2010 through time series Landsat images and phenology-based algorithms. Remote Sens. Environ. 160, 99–113.
Eagleson, P.S., Segarra, R.I., 1985. Water-limited equilibrium of savanna vegetation systems. Water Resour. Res. 21, 1483–1493.
Engle, D.M., Bidwell, T.G., Moseley, M.E., 1996. Invasion of Oklahoma Rangelands and Forests by Eastern Redcedar and Ashe Juniper. Oklahoma Cooperative Extension Service, Division of Agricultural Sciences and Natural Resources, Oklahoma State University.
Falkowski, M.J., Evans, J.S., Naugle, D.E., Hagen, C.A., Carleton, S.A., Maestas, J.D., Khalyani, A.H., Poznanovic, A.J., Lawrence, A.J., 2017. Mapping tree canopy cover in support of proactive prairie grouse conservation in Western North America. Rangel. Ecol. Manag. 70, 15–24.
FAO, 2012. Forest Resources Assessments (FRA2010). Food and Agricultural Organization of the United Nations, Rome.
Fredrickson, E.L., Estell, R.E., Laliberte, A., Anderson, D.M., 2006. Mesquite recruitment in the Chihuahuan Desert: historic and prehistoric patterns with long-term impacts. J. Arid Environ. 65, 285–295.
Gavier-Pizarro, G.I., Kuemmerle, T., Hoyos, L.E., Stewart, S.I., Huebner, C.D., Keuler, N.S., Radeloff, V.C., 2012. Monitoring the invasion of an exotic tree (*Ligustrum lucidum*) from 1983 to 2006 with Landsat TM/ETM plus satellite data and support vector machines in Cordoba, Argentina. Remote Sens. Environ. 122, 134–145.
Ge, J.J., Zou, C., 2013. Impacts of woody plant encroachment on regional climate in the southern Great Plains of the United States. J. Geophys. Res.-Atmos. 118, 9093–9104.
Gong, P., Wang, J., Yu, L., Zhao, Y.C., Zhao, Y.Y., Liang, L., Niu, Z.G., Huang, X.M., Fu, H.H., Liu, S., Li, C.C., Li, X.Y., Fu, W., Liu, C.X., Xu, Y., Wang, X.Y., Cheng, Q., Hu, L.Y., Yao, W.B., Zhang, H., Zhu, P., Zhao, Z.Y., Zhang, H.Y., Zheng, Y.M., Ji, L.Y., Zhang, Y.W., Chen, H., Yan, A., Guo, J.H., Yu, L., Wang, L., Liu, X.J., Shi, T.T., Zhu, M.H., Chen, Y.L., Yang, G.W., Tang, P., Xu, B., Giri, C., Clinton, N., Zhu, Z.L., Chen, J., Chen, J., 2013. Finer resolution observation and monitoring of global land cover: first mapping results with Landsat TM and ETM + data. Int. J. Remote Sens. 34, 2607–2654.
Grumbles, J., 1989. Control of eastern redcedar and ashe juniper with soil spot applications of picloram. In: Down to Earth. 45. pp. 13–16.
Hansen, M., Potapov, P., Moore, R., Hancher, M., Turubanova, S., Tyukavina, A., Thau, D., Stehman, S., Goetz, S., Loveland, T., 2013. High-resolution global maps of 21st-century forest cover change. Science 342, 850–853.
Hansen, M.C., Potapov, P.V., Goetz, S.J., Turubanova, S., Tyukavina, A., Krylov, A., Kommareddy, A., Egorov, A., 2016. Mapping tree height distributions in Sub-Saharan Africa using Landsat 7 and 8 data. Remote Sens. Environ. 185, 221–232.
Hibbard, K., Archer, S., Schimel, D., Valentine, D., 2001. Biogeochemical changes accompanying woody plant encroachment in a subtropical savanna. Ecology 82, 1999–2011.
Hughes, R.F., Archer, S.R., Asner, G.P., Wessman, C.A., McMurtry, C., Nelson, J., Ansley,

R.J., 2006. Changes in aboveground primary production and carbon and nitrogen pools accompanying woody plant encroachment in a temperate savanna. Glob. Chang. Biol. 12, 1733–1747.
Jones, M.D., Bowles, M.L., 2016. Eastern redcedar dendrochronology links hill prairie decline with decoupling from climatic control of fire regime and reduced fire frequency. J. Torrey Bot. Soc. 143, 239–253.
Knapp, A.K., Briggs, J.M., Collins, S.L., Archer, S.R., Bret-Harte, M.S., Ewers, B.E., Peters, D.P., Young, D.R., Shaver, G.R., Pendall, E., Cleary, M.B., 2008. Shrub encroachment in North American grasslands: shifts in growth form dominance rapidly alters control of ecosystem carbon inputs. Glob. Chang. Biol. 14, 615–623.
Kulmatiski, A., Beard, K.H., 2013. Woody plant encroachment facilitated by increased precipitation intensity. Nat. Clim. Chang. 3, 833–837.
Lassoie, J.P., Dougherty, P.M., Reich, P.B., Hinckley, T.M., Metcalf, C.M., Dina, S.J., 1983. Ecophysiological investigations of understory eastern redcedar in Central Missouri. Ecology 64, 1355–1366.
Maestas, J.D., Campbell, S.B., Chambers, J.C., Pellant, M., Miller, R.F., 2016. Tapping soil survey information for rapid assessment of sagebrush ecosystem resilience and resistance. Rangelands 38, 120–128.
Masek, J.G., Vermote, E.F., Saleous, N.E., Wolfe, R., Hall, F.G., Huemmrich, K.F., Gao, F., Kutler, J., Lim, T.K., 2006. A Landsat surface reflectance dataset for North America, 1990–2000. IEEE Geosci. Remote Sens. Lett. 3, 68–72.
McCulley, R.L., Jackson, R.B., 2012. Conversion of tallgrass prairie to woodland: consequences for carbon and nitrogen cycling. Am. Midl. Nat. 167, 307–321.
McKinley, D.C., Blair, J.M., 2008. Woody plant encroachment by *Juniperus virginiana* in a mesic native grassland promotes rapid carbon and nitrogen accrual. Ecosystems 11, 454–468.
Meddens, A.J.H., Hicke, J.A., Jacobs, B.F., 2016. Characterizing the response of pinon-juniper woodlands to mechanical restoration using high-resolution satellite imagery. Rangel. Ecol. Manag. 69, 215–223.
Meneguzzo, D.M., Liknes, G.C., 2015. Status and trends of eastern redcedar (*Juniperus virginiana*) in the central United States: analyses and observations based on forest inventory and analysis data. J. For. 113, 325–334.
Miettinen, J., Liew, S.C., 2011. Separability of insular Southeast Asian woody plantation species in the 50 m resolution ALOS PALSAR mosaic product. Remote Sens. Lett. 2, 299–307.
Mueller, H., Rufin, P., Griffiths, P., Siqueira, A.J.B., Hostert, P., 2015. Mining dense Landsat time series for separating cropland and pasture in a heterogeneous Brazilian savanna landscape. Remote Sens. Environ. 156, 490–499.
Munson, S.M., Webb, R.H., Housman, D.C., Veblen, K.E., Nussear, K.E., Beever, E.A., Hartney, K.B., Miriti, M.N., Phillips, S.L., Fulton, R.E., Tallent, N.G., 2015. Long-term plant responses to climate are moderated by biophysical attributes in a North American desert. J. Ecol. 103, 657–668.
Olofsson, P., Foody, G.M., Herold, M., Stehman, S.V., Woodcock, C.E., Wulder, M.A., 2014. Good practices for estimating area and assessing accuracy of land change. Remote Sens. Environ. 148, 42–57.
Pacala, S.W., Hurtt, G.C., Baker, D., Peylin, P., Houghton, R.A., Birdsey, R.A., Heath, L., Sundquist, E.T., Stallard, R.F., Ciais, P., Moorcroft, P., Caspersen, J.P., Shevliakova, E., Moore, B., Kohlmaier, G., Holland, E., Gloor, M., Harmon, M.E., Fan, S.M., Sarmiento, J.L., Goodale, C.L., Schimel, D., Field, C.B., 2001. Consistent land- and atmosphere-based US carbon sink estimates. Science 292, 2316–2320.
Pinno, B.D., Wilson, S.D., 2011. Ecosystem carbon changes with woody encroachment of grassland in the northern Great Plains. Ecoscience 18, 157–163.
Qin, Y., Xiao, X., Dong, J., Zhang, G., Shimada, M., Liu, J., Li, C., Kou, W., Moore, B., 2015. Forest cover maps of China in 2010 from multiple approaches and data sources: PALSAR, Landsat, MODIS, FRA, and NFI. ISPRS J. Photogramm. Remote Sens. 109, 1–16.
Qin, Y., Xiao, X., Wang, J., Dong, J., Ewing, K., Hoagland, B., Hough, D., Fagin, T., Zou, Z., Geissler, G., Xian, G., Loveland, T., 2016a. Mapping annual forest cover in sub-humid and semi-arid regions through analysis of Landsat and PALSAR imagery. Remote Sens. 8, 933.
Qin, Y.W., Xiao, X.M., Dong, J.W., Zhang, G.L., Roy, P.S., Joshi, P.K., Gilani, H., Murthy, M.S.R., Jin, C., Wang, J., Zhang, Y., Chen, B.Q., Menarguez, M.A., Biradar, C.M., Bajgain, R., Li, X.P., Dai, S.Q., Hou, Y., Xin, F.F., Moore, B., 2016b. Mapping forests in monsoon Asia with ALOS PALSAR 50-m mosaic images and MODIS imagery in 2010. Sci. Rep. 6.
Ratajczak, Z., Nippert, J.B., Briggs, J.M., Blair, J.M., 2014. Fire dynamics distinguish grasslands, shrublands and woodlands as alternative attractors in the Central Great Plains of North America. J. Ecol. 102, 1374–1385.
Saintilan, N., Rogers, K., 2015. Woody plant encroachment of grasslands: a comparison of terrestrial and wetland settings. New Phytol. 205, 1062–1070.
Sankey, T.T., Germino, M.J., 2008. Assessment of juniper encroachment with the use of satellite imagery and geospatial data. Rangel. Ecol. Manag. 61, 412–418.
Schmidt, T.L., Leatherberry, E.C., 1995. Expansion of eastern redcedar in the lower Midwest. North. J. Appl. For. 12, 180–183.
Shimada, M., Ohtaki, T., 2010. Generating large-scale high-quality SAR mosaic datasets: application to PALSAR data for global monitoring. IEEE J. Sel. Top. Appl. Earth Obs. Remote Sens. 3, 637–656.
Shimada, M., Isoguchi, O., Tadono, T., Isono, K., 2009. PALSAR radiometric and geometric calibration. IEEE Trans. Geosci. Remote Sens. 47, 3915–3932.
Shimada, M., Itoh, T., Motooka, T., Watanabe, M., Shiraishi, T., Thapa, R., Lucas, R., 2014. New global forest/non-forest maps from ALOS PALSAR data (2007–2010). Remote Sens. Environ. 155, 13–31.
Smith, A.M.S., Strand, E.K., Steele, C.M., Hann, D.B., Garrity, S.R., Falkowski, M.J., Evans, J.S., 2008. Production of vegetation spatial-structure maps by per-object analysis of juniper encroachment in multitemporal aerial photographs. Can. J. Remote. Sens. 34, S268–S285.
Staff, S.S., 2016a. Grid Soil Survey Geographic (gSSURGO) Database for the United States of America and the Territories, Commonwealths, and Island Nations served by the USDA-NRCS. United States Department of Agriculture, Natural Resources Conservation Service(Available online at http://datagateway.nrcs.usda.gov/. (FY2016 offical release)).
Staff, S.S., 2016b. The Gridded Soil Survey Geographic (SSURGO) Database for Oklahoma. United States Department of Agriculture, Natural Resources Conservation Service(Available online at http://datagateway.nrcs.usda.gov/, (FY2016 official release)).
Strand, E.K., Robinson, A.P., Bunting, S.C., 2007. Spatial patterns on the sagebrush steppe/western juniper ecotone. Plant Ecol. 190, 159–173.
Symeonakis, E., Higginbottom, T., 2014. Bush encroachment monitoring using multi-temporal Landsat data and random forests. Int. Arch. Photogramm. Remote. Sens. Spat. Inf. Sci. 1, 29–35.
Tucker, C.J., 1979. Red and photographic infrared linear combinations for monitoring vegetation. Remote Sens. Environ. 8, 127–150.
Van Auken, O.W., 2009. Causes and consequences of woody plant encroachment into western North American grasslands. J. Environ. Manag. 90, 2931–2942.
Van Auken, O., Bush, J., 2013. Encroachment and Secondary Succession. Invasion of Woody Legumes. Springer, pp. 11–14.
Vermote, E.F., ElSaleous, N., Justice, C.O., Kaufman, Y.J., Privette, J.L., Remer, L., Roger, J.C., Tanre, D., 1997. Atmospheric correction of visible to middle-infrared EOS-MODIS data over land surfaces: background, operational algorithm and validation. J. Geophys. Res.-Atmos. 102, 17131–17141.
Walker, T.L., Hoback, W.W., 2007. Effects of invasive eastern redcedar on capture rates of *Nicrophorus americanus* and other Silphidae. Environ. Entomol. 36, 297–307.
Wang, J., Xiao, X.M., Wagle, P., Ma, S.Y., Baldocchi, D., Carrara, A., Zhang, Y., Dong, J.W., Qin, Y.W., 2016. Canopy and climate controls of gross primary production of Mediterranean-type deciduous and evergreen oak savannas. Agric. For. Meteorol. 226, 132–147.
Wang, J., Xiao, X., Qin, Y., Dong, J., Geissler, G., Zhang, G., Cejda, N., Alikhani, B., Doughty, R.B., 2017. Mapping the dynamics of eastern redcedar encroachment into grasslands during 1984–2010 through PALSAR and time series Landsat images. Remote Sens. Environ. 190, 233–246.
Ward, D., Hoffman, M.T., Collocott, S.J., 2014. A century of woody plant encroachment in the dry Kimberley savanna of South Africa. Afr. J. Range Forage Sci. 31, 107–121.
Weisberg, P.J., Lingua, E., Pillai, R.B., 2007. Spatial patterns of pinyon-juniper woodland expansion in central Nevada. Rangel. Ecol. Manag. 60, 115–124.
Weng, E.S., Luo, Y.Q., 2008. Soil hydrological properties regulate grassland ecosystem responses to multifactor global change: a modeling analysis. J. Geophys. Res. Biogeosci. 113.
Wigley, B.J., Bond, W.J., Hoffman, M.T., 2010. Thicket expansion in a South African savanna under divergent land use: local vs. global drivers? Glob. Chang. Biol. 16, 964–976.
Williams, R.J., Hallgren, S.W., Wilson, G.W.T., Palmer, M.W., 2013. *Juniperus virginiana* encroachment into upland oak forests alters arbuscular mycorrhizal abundance and litter chemistry. Appl. Soil Ecol. 65, 23–30.
Wine, M.L., Ochsner, T.E., Sutradhar, A., Pepin, R., 2012. Effects of eastern redcedar encroachment on soil hydraulic properties along Oklahoma's grassland-forest ecotone. Hydrol. Process. 26, 1720–1728.
Wulder, M.A., White, J.C., Goward, S.N., Masek, J.G., Irons, J.R., Herold, M., Cohen, W.B., Loveland, T.R., Woodcock, C.E., 2008. Landsat continuity: issues and opportunities for land cover monitoring. Remote Sens. Environ. 112, 955–969.
Wulder, M.A., Masek, J.G., Cohen, W.B., Loveland, T.R., Woodcock, C.E., 2012. Opening the archive: how free data has enabled the science and monitoring promise of Landsat. Remote Sens. Environ. 122, 2–10.
Wulder, M.A., White, J.C., Loveland, T.R., Woodcock, C.E., Belward, A.S., Cohen, W.B., Fosnight, E.A., Shaw, J., Masek, J.G., Roy, D.P., 2016. The global Landsat archive: status, consolidation, and direction. Remote Sens. Environ. 185, 271–283.
Xiao, X.M., Boles, S., Liu, J.Y., Zhuang, D.F., Frolking, S., Li, C.S., Salas, W., Moore, B., 2005. Mapping paddy rice agriculture in southern China using multi-temporal MODIS images. Remote Sens. Environ. 95, 480–492.
Xiao, X., Hagen, S., Zhang, Q., Keller, M., Moore, B., 2006. Detecting leaf phenology of seasonally moist tropical forests in South America with multi-temporal MODIS images. Remote Sens. Environ. 103, 465–473.
Xiao, X., Biradar, C.M., Czarnecki, C., Alabi, T., Keller, M., 2009. A simple algorithm for large-scale mapping of evergreen forests in Tropical America, Africa and Asia. Remote Sens. 1, 355–374.
Zhong, L.H., Gong, P., Biging, G.S., 2014. Efficient corn and soybean mapping with temporal extendability: a multi-year experiment using Landsat imagery. Remote Sens. Environ. 140, 1–13.
Zhu, Z., Woodcock, C.E., 2012. Object-based cloud and cloud shadow detection in Landsat imagery. Remote Sens. Environ. 118, 83–94.
Zou, C.B., Turton, D.J., Will, R.E., Engle, D.M., Fuhlendorf, S.D., 2014. Alteration of hydrological processes and streamflow with juniper (*Juniperus virginiana*) encroachment in a mesic grassland catchment. Hydrol. Process. 28, 6173–6182.
Zou, C.B., Qiao, L., Wilcox, B.P., 2016. Woodland expansion in central Oklahoma will significantly reduce streamflows - a modelling analysis. Ecohydrology 9, 807–816.

Annual Maps of Eastern Redcedar Forests in Oklahoma during 1984-2010 at 30-m Resolution from Landsat and PALSAR Images

Summary

Woody plant encroachment in grasslands has been rapidly increasing in Oklahoma. The researchers at the Earth Observation and Modeling Facility, University of Oklahoma carried out a pilot project to map and report the dynamics of eastern redcedar forest encroachment at 5-year interval (epoch) from 1984 to 2010 in Oklahoma.

Data and Methods

We use images from PASAR at 25-m spatial resolution in 2010 and Landsat TM and ETM+ at 30-m spatial resolution during 1984-2010. Detailed information on the eastern redcedar forest mapping algorithm and annual maps of eastern redcedar forests are reported in Wang et al., (2017).

Provisional Data Product for Eastern RedCedar Forests during 1984 - 2010

Figure 1 shows the spatial-temporal dynamics of eastern redcedar forests in Landsat P28/R35 tile

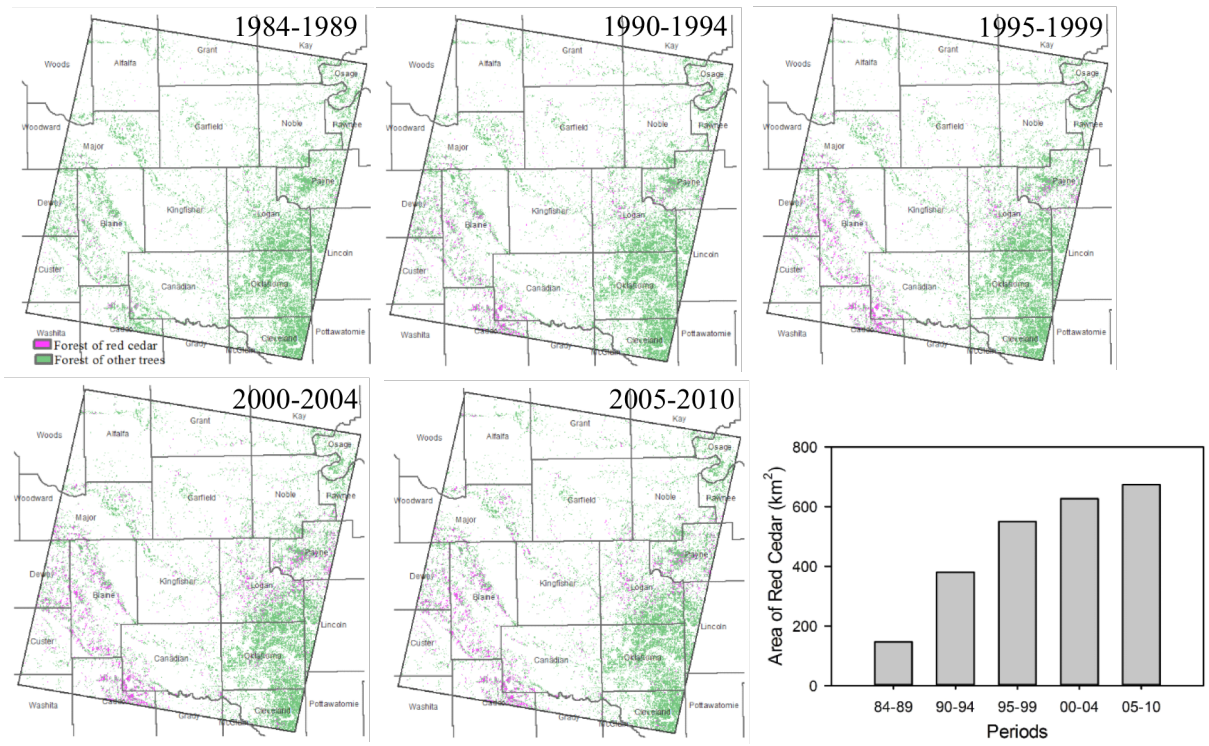

Figure 1. Spatial-temporal dynamics of red cedar during 1984-2010 at 30-m spatial resolution

Reference

Wang, J., *et al*., 2017, Mapping the dynamics of eastern redcedar encroachment into grasslands during 1984-2010 through PALSAR and time series Landsat images, *Remote Sensing of Environment*, 190: 233-246.

Contact Information

Prof. Xiangming Xiao (xiangming.xiao@ou.edu); (405) 325-8941 (Office)
Department of Microbiology and Plant Biology, Center for Spatial Analysis, University of Oklahoma; please visit Earth Observation and Modeling Facility http://www.eomf.ou.edu.